

A novel pathway for efficient characterisation of additively manufactured thermoplastic elastomers



Rhosslyn Adams^a, Shwe P. Soe^a, Rafael Santiago^b, Michael Robinson^a, Benjamin Hanna^a, Graham McShane^d, Marcílio Alves^c, Roy Burek^{a,e}, Peter Theobald^{a,*}

^a Cardiff School of Engineering, Cardiff University, UK

^b Centre of Engineering, Modelling and Applied Social Science (CECS), Federal University of ABC (UFABC), Brazil

^c Department of Mechatronics and Mechanical Systems Engineering, Group of Solid Mechanics and Structural Impact, University of São Paulo (USP), Brazil

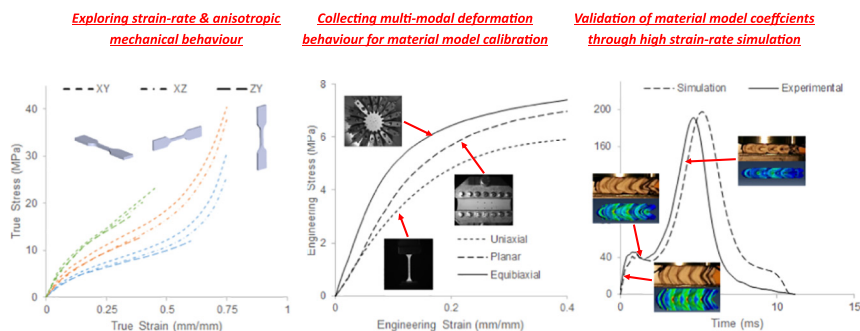
^d Department of Engineering, Trumpington Street, Cambridge University, UK

^e Charles Owen, Royal Works, Croesfoel Industrial Park, Wrexham, UK

HIGHLIGHTS

- Established a novel pathway to efficiently calibrate a material model for additively manufactured thermoplastic elastomers
- New pathway is the first that captures the hyperelastic and linear viscoelastic behaviour within a dynamic environment
- Validity demonstrated by comparing the experimental and simulated behaviour of a lattice structure at high strain-rates
- Introduction of this pathway to efficient characterisation of this AM material type removes a barrier to use industry

GRAPHICAL ABSTRACT



ARTICLE INFO

Article history:

Received 11 April 2019

Received in revised form 3 June 2019

Accepted 4 June 2019

Available online 6 June 2019

Keywords:

Thermoplastic elastomer

Polymer characterisation

Hyperelastic

Viscoelastic

High strain-rate FEA analysis

Laser sintering

Data availability:

The raw/processed data required to reproduce these findings cannot be shared at this time as the data also forms part of an ongoing study.

ABSTRACT

Thermoplastic elastomers (TPE) are commonly used to fabricate structures for application in repeatable, energy absorption environments. The emergence of additive manufacturing (AM) means scope now exists to design and build complex TPE components that can mechanically outperform traditionally manufactured equivalents. The ability to efficiently characterize these new TPE AM materials is, however, a barrier preventing wider industrial uptake. This study aims to establish a novel pathway for efficiently characterizing materials used in transient, dynamic applications, to ultimately enable accurate finite element (FE) simulation. A laser sintered TPE powder was characterised by performing low, intermediate and high rate uniaxial tension tests, plus planar and equibiaxial loading states. These data demonstrated significantly different behaviour across strain rates and deformation modes, necessitating fit of an augmented hyperelastic and linear viscoelastic model. FE software was then used to calibrate material model coefficients, with their validity evaluated by comparing the simulated and experimental behaviour of the material in isolated (uniaxial tensile) and mixed modal (lattice-based impact) deformation states. Close correlation demonstrated this novel approach efficiently generated valid material model coefficients, removing a barrier to industry adopting these materials. This creates opportunity to exploit these new technologies for the design optimization and fabrication of high-performance components.

© 2019 The Authors. Published by Elsevier Ltd. This is an open access article under the CC BY license (<http://creativecommons.org/licenses/by/4.0/>).

* Corresponding author.

E-mail address: TheobaldPS@Cardiff.ac.uk (P. Theobald).

1. Introduction

Thermoplastic elastomers (TPEs) can undergo large regimes of elastically recoverable strain and exhibit negligible creep [1], demonstrating their functional value when compared to other polymers and especially those used in repeated, energy-absorbing applications. TPE components are typically fabricated via extrusion or injection moulding, requiring high capital investment and yet affording limited design freedom. Awareness is now increasing of the potential mechanical advantages afforded by utilising additive manufacturing (AM) to achieve complex, three-dimensional TPE geometries [2–5].

Laser sintering (LS) is an AM technique that fabricates parts by fusing powder-based material over successive layers [6,7,8]. The self-supporting nature of such processes provides opportunity to create complex structures from polymers, metals, ceramics and composites [9]. Polyamide [10,11] and polypropylene [12] are commonly used polymeric powders, though the inability of the sintered material to undergo large deformation regimes inherently limits final part functionality. Greater design freedom is now attainable via the emergence of TPE LS powders [13–15], enabling creation of high-performance components including for use in repeated, energy absorbing (i.e. high strain rate) applications [16].

Accurate FE simulations are possible for design-optimising TPE AM parts used within static applications for optimisation [17,18]. The industrial uptake for using TPE AM powders in dynamic environment is limited, however, the need to accurately simulate the hyperelastic, viscoelastic and anisotropic behaviours exhibited within high strain-rate environments require multi-modal characterisation, i.e. measures including Young's Modulus and Poisson's ratio are insufficient [19]. Efficiently achieving this characterisation and validation requires a methodology that draws directly on data that quantifies these behaviours, enabling generation of coefficients for established material models for input into FE software [20]. To date, however, no such pathway is described in the literature. Previous work has described the validation of hyperelastic and viscoelastic material model coefficients via the fabrication, experimental and computational investigation of an AM honeycomb structure [21]. This approach, whilst successful, did not fully assess the robustness of the established model coefficients, by validating in an isolated deformation state at multiple strain rates. A need still exists, therefore, to establish an efficient characterisation pathway, removing a barrier for industrial adoption and unlocking the potential afforded by TPE AM design.

This study aims to establish a novel pathway for the efficient characterisation of TPE AM materials, generating valid material model coefficients that will allow accurate FE simulations within a transient, dynamic loading environment. Validation will be achieved by presenting data describing simulated and experimental isolated (uniaxial tension) and mixed deformation (lattice-based impact) behaviour. This outcome will provide a foundation for developing high-performance TPE AM components, enabling industry to exploit the potential of these emerging technologies.

2. Materials & methods

2.1. Materials

This study investigated a commercially available LS TPE powder (Luvosint X92A-1, Lehmann & Voss & Co; Hamburg, Germany). Manufacturing was sub-contracted to a 3rd party (FKM; Biedenkopf, Germany), selected for their AM polymer processing expertise. Mechanical test coupons were designed in-house using commercially available software (Solidworks; Dassault Systems, France), to enable material characterisation. The dynamic tensile loading coupons for different strain rates were adopted from the relevant design standards, as described in Section 2.2.1.

2.2. Methods

2.2.1. Experimental testing of material anisotropy and rate sensitivity

Tensile tests were performed at low, intermediate and high strain rates nominally equivalent to 0.05/s, 5/s and 100/s respectively, to investigate the rate sensitivity of the LS TPE material. Coupon gauge-length designs were dependant on the testing rates, as per ASTM-638 [22] (0.05/s = 33 mm; 5/s = 5 mm, 100/s = 22 mm) (Fig. 1(a)). Additional coupon designs were manufactured ($n = 3$) in 3 orthogonal build orientations, with sintered layers lying through-thickness (xy), width (xz) and length (zy) (Fig. 1(b)).

Low strain rate testing ($\sim 0.05/s$) was performed using a universal testing machine (Instron 3369; Instron, Massachusetts, US), with each coupon loaded to failure as per ASTM-638. Specimen strain was measured with video extensometry (VIC-2D; Correlated Solution, Columbia, US). Intermediate strain rate testing ($\sim 5/s$) was performed using a faster uniaxial testing machine (ElectroPulse E1000; Instron, Massachusetts, US), whilst high strain rate ($\sim 100/s$) used an in-house rig that achieves the highest rate via a falling mass [23]. Strain versus falling mass displacement was constantly monitored, to ensure a constant strain rate in the regions of interest. The intermediate and high strain testing coupons had a high-contrast black-white speckle pattern applied to the surface prior to testing, to enable strain measurements via digital image correlation (DIC) (Photron SA-5; Photron, Tokyo, Japan).

2.2.2. Experimental characterisation for material modelling

Quasistatic uniaxial, planar and equibiaxial tension deformation mode data was collected to define the hyperelastic (HE) behaviour, with uniaxial stress relaxation data collected to define the linear viscoelastic (LVE) behaviour, in the range 0–0.5 mm/mm strain. Data collected for material model calibration is representative of material printed in the 'xy' build orientation.

2.2.2.1. Uniaxial tension. Testing was performed using an electromechanical uniaxial testing machine (Zwick Z50; Ulm, Germany), fitted with a 1kN load cell and non-slip grips following ISO 37 [24], using a reduced crosshead speed (100 mm/min) to minimise the effect of strain rate sensitivity (Fig. 2(a)). Test coupons were designed and fabricated as per tensile testing specimen type 1. Non-contact video extensometry (iMetrum CAM028; Bristol, UK) enabled strain measurement within the gauge length.

2.2.2.2. Planar tension (pure shear). An in-house jig (Fig. 2(b)) was designed to apply load to a wide sheet of material, achieving a 10-fold width-to-height gauge area ratio [1]. It was clamped within an electromechanical uniaxial testing machine (Zwick Z50; Ulm, Germany), fitted with a 50kN load cell. Planar tension coupons (60 × 200 × 2 mm) had aluminium strips (20 × 200 mm) affixed across the top and bottom using industrial-strength epoxy, providing a non-slip boundary and ensuring clamping pressure is even distributed when mounted in the jig jaws. Specimen strain was measured with video extensometry across 3 distinct pairs of strain locations, with similarity indicating homogeneous strain.

2.2.2.3. Equibiaxial tension. Testing was performed using an in-house jig (Fig. 2(c)), designed specifically to achieve multi-axial loading via a uniaxial testing machine [21]. Coupons were circular shaped (50 mm dia, 2 ± 0.15 mm thickness), with the perimeter comprising 16 clamping-tabs. A series of cuts and radii-edges ensured a homogenous circular strain region, reducing the contribution of stress concentrations and mitigating premature specimen failure. Coupons were then secured in the jig which, in turn, was loaded into an electromechanical uniaxial testing machine (Zwick Z50; Ulm, Germany) fitted with a 50kN load. A 100 mm/min strain rate was applied in two directions, with machine-recorded load data retrospectively converted into equibiaxial stress. Non-contact video extensometry was again used to measure the

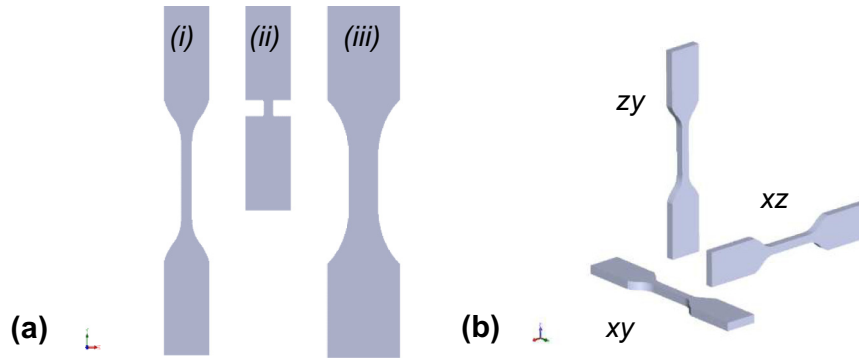


Fig. 1. (a) Coupon variants for mechanical performance tensile tests for (i) low, (ii) intermediate and (iii) high strain rates. (b) Coupon build orientation.



Fig. 2. Multi deformation-mode mechanical characterisation in (a) uniaxial, (b) planar and (c) equibiaxial tension.

specimen strain across 4 distinct pairs of strain locations, with similarity indicating a state of homogenous strain.

2.2.2.4. Single step stress relaxation testing. The tensile test geometry was used to measure stress relaxation. The single-step extension was performed at the maximum available cross-head speed (600 mm/min), to a strain of 0.5 and followed by a 100 s relaxation period. For solid elastomers it is well established that the bulk modulus, which captures the volumetric behaviour, does not exhibit time-dependence; hence, a uniaxial tensile test can be used instead of a pure shear test, as normalised Young's modulus and Shear modulus against time are considered equivalent. For the basis of representing the time-dependent behaviour, a LVE model is convenient where normalised stress relaxation behaviour is sufficient to calibrate a model.

2.2.3. Material modelling for finite element implementation

2.2.3.1. Hyperelastic material modelling. Material model coefficients were captured to describe the TPE's non-linear elastic behaviour, in a manner suitable for implementation in a commercial FE software. This was calculated from multi deformation-mode data, collected using the methodology detailed in Section 2.2.1. The following hyperelastic strain energy potentials were considered utilising the Abaqus in-built solver: Ogden N1 through N6, Reduced Polynomial N = 3 through N = 6, Arruda-Boyce and Van Der Waals for the range of 0 to 0.5 strain.

The relative difference between the model output and the experimental data was calculated to quantitatively compare the suitability of each model. The relative difference was summed for each individual deformation mode (Eq. (1)), in addition to all variants of strain-mode combinations. The most appropriate model minimised the total relative difference, with a lower value indicating a better fit.

$$Relative\ difference = \frac{\int_{\epsilon_{min}}^{\epsilon_{max}} |\sigma_{mod} - \sigma_{exp}| d\epsilon}{\int_{\epsilon_{min}}^{\epsilon_{max}} \sigma_{exp} d\epsilon} \quad (1)$$

where σ_{exp} and σ_{model} are stress for experimental and material model data respectively, and ϵ is the applied strain.

2.2.3.2. Viscoelastic material modelling. The TPE's time-dependant behaviour was captured using material model coefficients suitable for implementation in a commercial FE software. Normalised stress relaxation data was calculated using the methodology detailed in Section 2.2.1. The Prony series, a sum of exponential terms as detailed by Eq. (2), was used to represent the linear viscoelastic behaviour. The Abaqus in-built solver was used to perform a curve fitting procedure, utilising a non-linear least squares fit with an allowable average root-mean-square error value of 0.001, before calculating a set of series coefficients.

$$g_R(t) = 1 - \sum_{i=1}^N g_i^p \left(1 - e^{-\frac{t}{\tau_i^G}} \right) \quad (2)$$

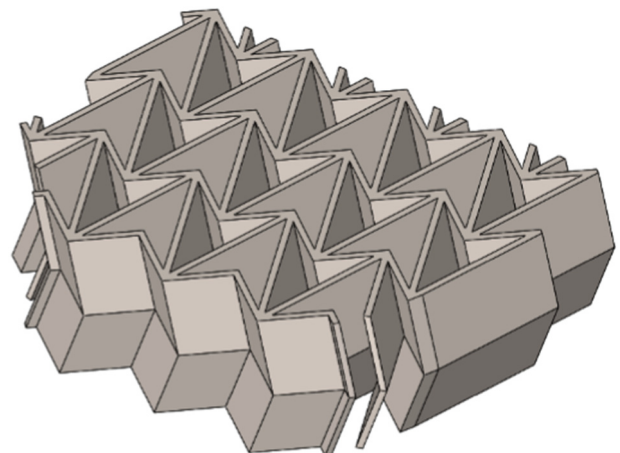


Fig. 3. Computational model of the 'MO' lattice visualised using Solidworks.

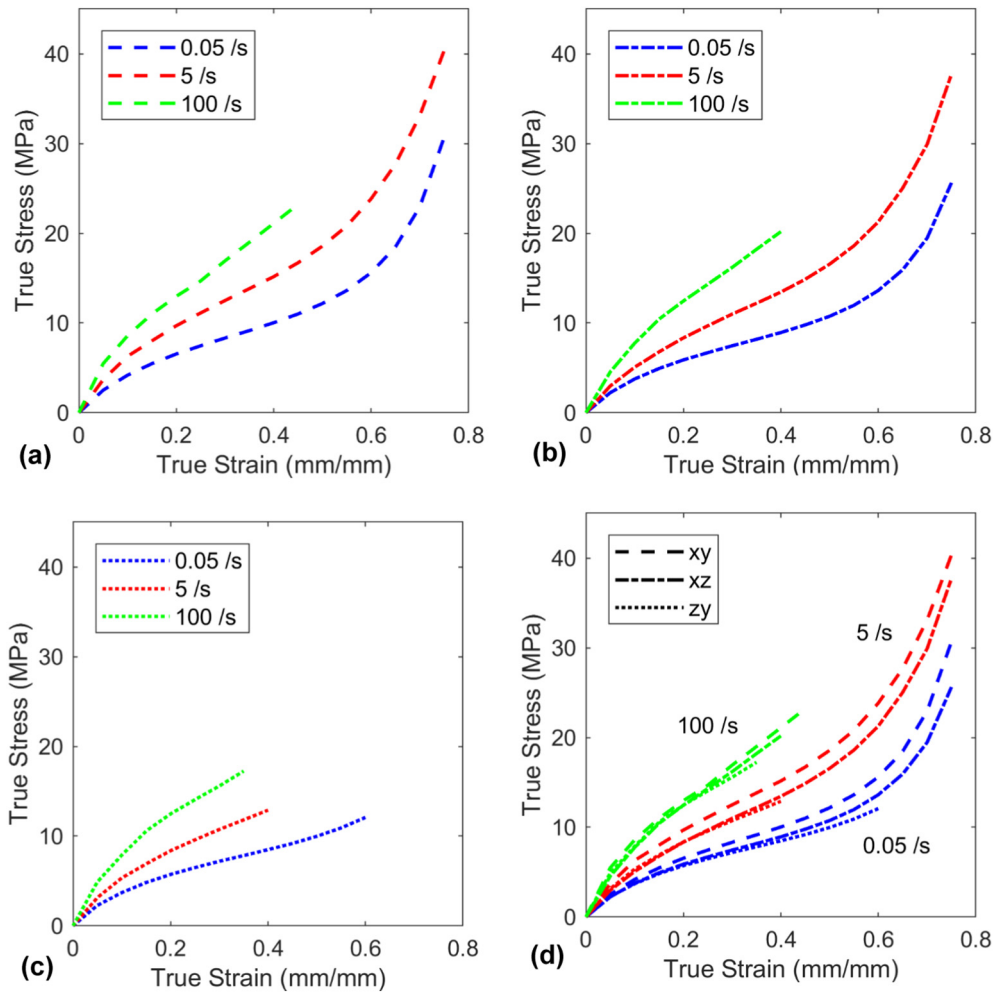


Fig. 4. Mechanical response of LS TPE under uniaxial tension at different strains rates for build orientation (a) 'xy', (b) 'xz', (c) 'zy' and (d) comparison of build orientation relative to strain rate.

where N , \bar{g}_i^p and τ_i , $i = 1, 2, \dots, N$ are material constants of the prony series expansion.

2.2.4. Finite element analysis

2.2.4.1. Dynamic tensile loading. Dynamic tensile loading was simulated using Abaqus/Explicit, to examine and validate the proposed material model in an isolated deformation mode (i.e. uniaxial tension) at the high strain rate utilised for testing in Section 2.2.1. The Abaqus solver enabled consideration of large deformation effect. A single unit mesh was simulated, which ensured a pure state of uniaxial tension for comparison against experimental data. The lower edge of the cell was restrained in the y -direction to simulate non-slip grips, whilst the gauge length was able to freely deform and constrict in all three orthogonal directions. To simulate deformation, deformation-time history recorded from the experimental test (Section 2.2.1) was applied to the upper section by means of a displacement and amplitude boundary condition.

2.2.4.2. Dynamic impact loading. Dynamic linear impacts were simulated using Abaqus/Explicit, to examine and validate the proposed material model in a mixed deformation mode and varying strain rates. An established lattice structure, which has been previously reported for energy-absorption, was selected from the literature [25]. This comprised a series of stacked sheets of the Miura-ori folding pattern (Fig. 3) [26], hereafter referred to as the 'MO' lattice. The folding nature of this structure under dynamic compression induces a mixed state of

deformation (i.e. uniaxial, planar and equibiaxial tension), meaning it is a demanding structure to evaluate the validity and robustness of the new material model coefficients.

The Abaqus/Explicit solver enabled consideration of large deformation effects and complex self-contact interactions that are present during 'MO' lattice compression. Prior to investigation, the computational geometry was modified by an averaged factor in two axes, to compensate for the thermal shrinkage induced by laser sintering (see below section). The modified 'MO' lattice computational geometry was then imported into Abaqus CAE and placed between two rigid plates. A 1 mm global seed was proliferated to construct a mesh, following a convergence test. An eight-node brick element with reduced integration (C3D8R) and hourglass control active was utilised, with hexahedron shape type. The upper plate was assigned a 4.7 kg point mass and prescribed pre-impact velocities of nominally 2 m/s, 3 m/s and 4 m/s – equivalent to strain rates of 80/s, 120/s and 160/s respectively. The acceleration-time history was extracted from a reference node at the centre of the upper rigid plate, for comparison with mechanical testing results.

2.2.5. Experimentation for material model validation

Impact testing, to validate the results of the FE simulation, was performed on a monorail shock absorption testing facility (model: 1002 MAU1006/CF/ALU; AD Engineering, Bergamo, Italy). The MO structure was fabricated using the above LS TPE powder and 3rd party contractor. Shrinkage, relative to the CAD geometry, was measured using a digital

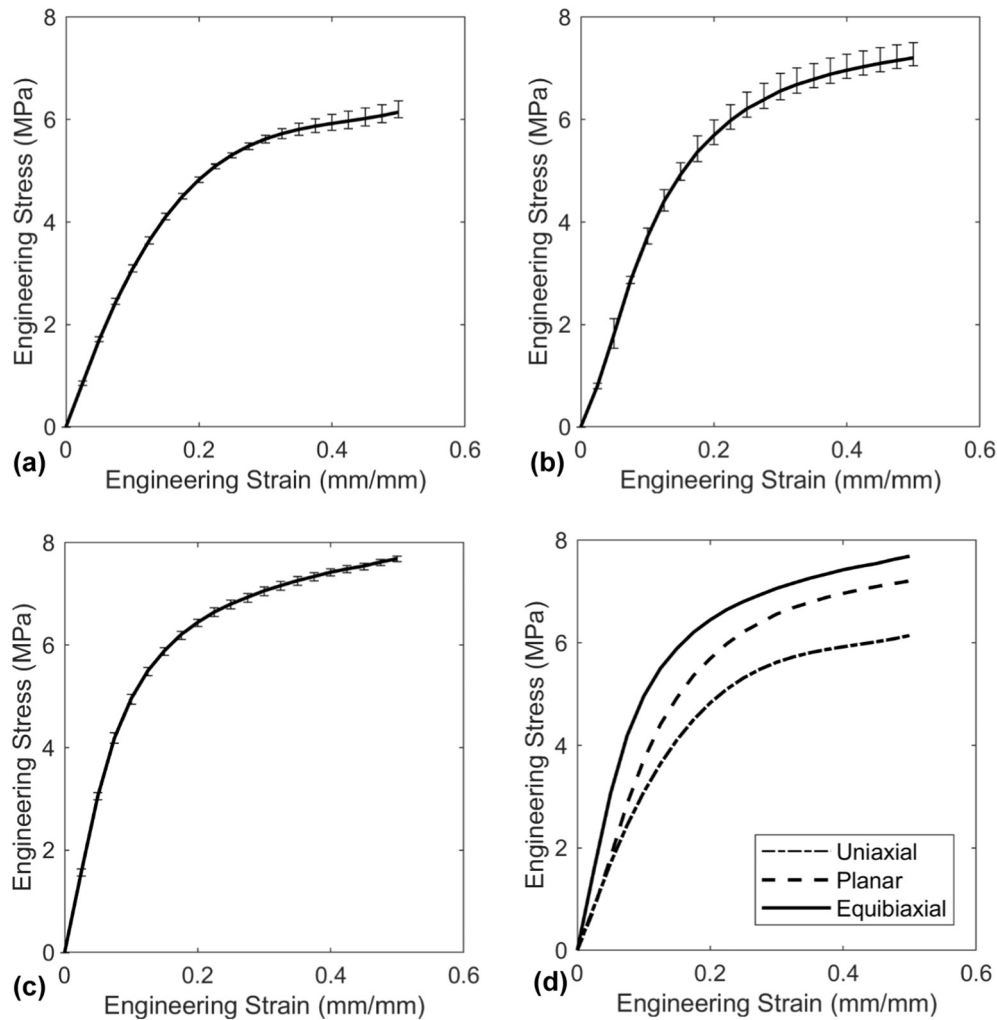


Fig. 5. Experimental data for multi deformation-mode behaviour: (a) uniaxial, (b) planar, (c) equibiaxial tension and (d) combined for comparison.

Vernier Caliper (Absolute AOS Digimatic, Mitutoyo, Japan). The 'xy' axis was quantified by the change in wall thickness, whilst 'z' was measured by the overall change in height of the specimen. Impact data was then collected via a single axis accelerometer (model: PCB353/B17-1D, 500 g maximum acceleration), located in-line with the centre impact platen and recorded at 50 kHz via a data acquisition system (model: 'DLS 9000/CM 625'; AD Engineering, Bergamo, Italy). Data was filtered in accordance with ISO 6487 class 1000. The 'MO' lattice specimen was taped in the centre of the fixed lower platen of 130 mm diameter. A separate, flat 4.7 kg impacting platen of 130 mm diameter was then wire-guided, under free-fall, on to the sample. The sample was subjected to impact velocities of 2 m/s, 3 m/s and 4 m/s independently-equivalent to strain rates of 80/s, 120/s and 160/s respectively, with sufficient time allowed to reduce the effect of stress relaxation.

3. Results

3.1. Experimental testing of material anisotropy and rate sensitivity

Uniaxial tension data for the LS TPE coupons tested at three different strain rates and printed in three orthogonal build directions, are presented in Fig. 4. Coupons were strained to failure, with true stress calculated from the effective change in specimen cross-sectional area measured via DIC.

3.1.1. Strain rate sensitivity

Strain rate sensitivity is demonstrated in Fig. 4(a)–(c), with markedly different responses evident at low, intermediate and high strain-rates. At increasing strain-rates, higher levels of true stress for equivalent levels of true strain are observed, e.g. at a true strain of 0.35, the high strain rate true stress is 2.1–2.2 times greater than the equivalent true stress under intermediate strain rate, and 1.4–1.5 under low strain rate. Additionally, the ultimate true strain decreased by a factor of 0.7 for intermediate, compared to low, strain rate testing. For high strain-rate testing, specimen failure could not be achieved due to limitations of the testing equipment; hence, the ultimate true strain at this strain rate is unknown.

3.1.2. Build orientation sensitivity

Build orientation sensitivity is demonstrated in Fig. 4(d). It is evident that the build orientation of a LS TPE has a significant effect on overall mechanical performance. Coupons built in the 'xy' direction demonstrated the greatest true stress-to-failure and true strain-to-failure when compared to 'xz' and 'zy'.

3.2. Material model development and calibration

3.2.1. Experimental characterisation

Uniaxial, planar and equibiaxial tension data for the LS TPE manufactured in the 'xy' orientation are presented in Fig. 5. Coupons

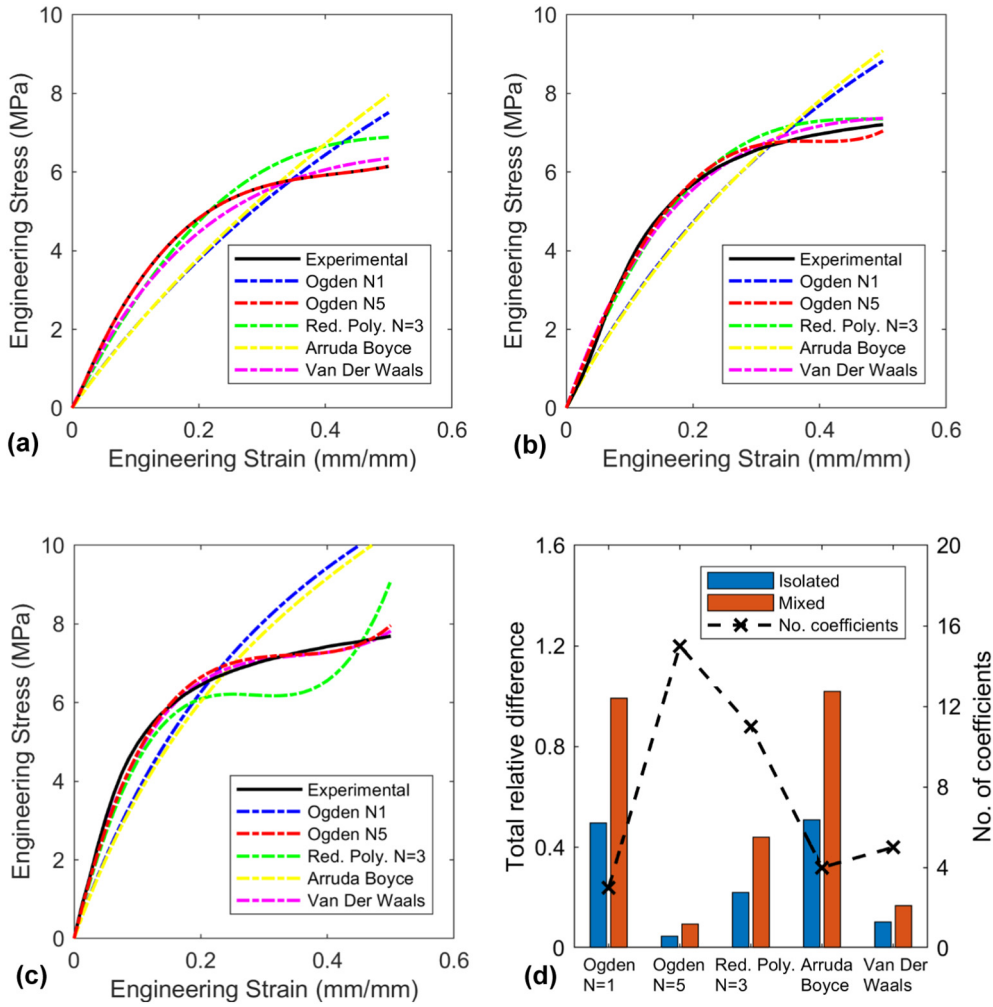


Fig. 6. Comparison of hyperelastic material models: (a) uniaxial, (b) planar, (c) equibiaxial tension and (d) comparison of total relative difference and number of coefficients for each model.

were strained to 0.5 mm/mm, with engineering stress calculated from the applied load and initial cross-section dimensions. Behaviour was characteristically linear in the range 0–0.1 strain. The initial modulus for uniaxial, planar and equibiaxial tension was calculated as 30.86, 37.13 and 49.58 MPa, respectively. At a nominal engineering strain of 0.5, tensile stress was 6.14 MPa, planar shear stress was 7.21 MPa and equibiaxial stress was 7.69 MPa.

3.2.2. Hyperelastic material model calibration

Experimental test data was fitted to the hyperelastic constitutive models available in Abaqus. Fig. 6(a)–(c) presents each viable material model, i.e. those that achieved a stable state for all strains ranging between 0 and 0.5. Unstable material models were excluded and so are omitted from the plot. Experimental data are presented for comparison

Table 1
Hyperelastic material model, Ogden N = 5, coefficients for implementation in commercially available FE software.

	Mu _I	Alpha _I	D _I
1	903.004544	3.71988736	0
2	-723.556424	5.23968936	0
3	264.028331	6.18711358	0
4	-669.431935	2.26365354	0
5	236.657210	1.41521537	0

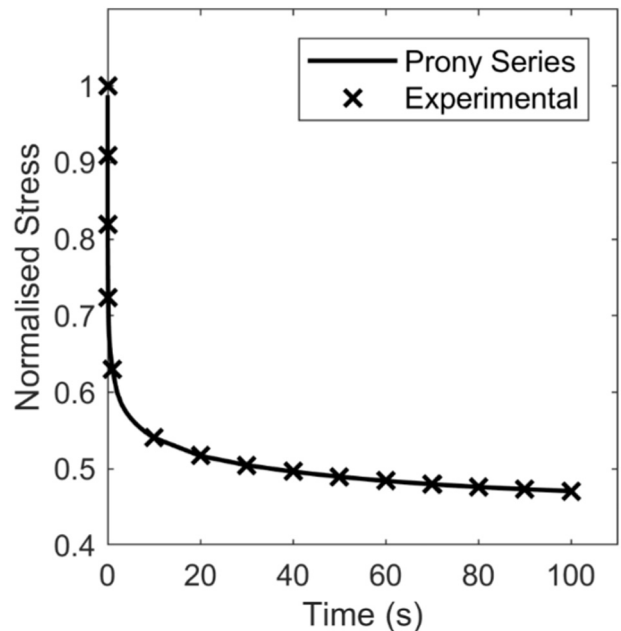


Fig. 7. Normalised stress relaxation test data Prony series representation.

Table 2

Linear viscoelastic material model, Prony series, coefficients for implementation in commercially available FE software.

	G ₁	K ₁	Tau ₁
1	0.1645	0	1.35E-03
2	0.13196	0	7.13E-02
3	8.98E-02	0	0.91852
4	7.29E-02	0	6.2708
5	8.04E-02	0	49.41

where varying degrees of agreement are observed. Models that achieved stability for all strains were: Ogden $N = 1$ & $N = 5$, Reduced Polynomial $N = 3$ (Yeoh), Van Der Waals, and Arruda-Boyce.

The different material models were evaluated by calculating the relative difference between the model output and experimental dataset (Fig. 6(d)). The relative difference was calculated for each independent deformation mode and coupled deformation modes, to determine efficacy at assessing multi-modal deformation loading scenarios. In both cases, the Ogden $N = 5$ model presented the best fit to experimental data, with a relative error of 0.048 and 0.095, respectively. Coefficients for this hyperelastic material model are presented in Table 1, with the model becoming increasingly inaccurate outside the predicted strain range.

3.2.3. Linear viscoelastic material model calibration

Normalised single-step stress relaxation test data was fitted to the linear viscoelastic constitutive model available in Abaqus (Prony series). Fig. 7 presents the normalised experimental data against the Prony series representation which, due to the specific low root means square (RMS) error prescribed by the solver (0.001), is calibrated closely to the experimental data. Examining the experimental data trend enables estimation of a long-term normalised modulus equal to 0.5. The Prony series coefficients that define the curve presented in Fig. 7 are quantified in Table 2.

3.3. Finite element validation

3.3.1. Dynamic tensile loading

Comparison of the experimental and simulated results is presented in Fig. 8, to assess the efficacy of the material model in a dynamic single state of deformation. Generally, simulations demonstrate fair predictions.

3.3.2. Dynamic impact loading

Comparison of the experimental and simulated results is presented in Fig. 9. Data describing the dynamic impact attributes, including peak acceleration, time to peak and pulse duration, were evaluated to assess the efficacy of the material model in a dynamic mixed deformation mode at several strain rates. Experimental and simulated peak acceleration, time to peak and pulse duration were all within 15% for each impact velocity, except for 2 m/s impact where the time to peak was 40%. Fig. 10 presents the similarity of the deformation kinematics between experimental and simulation, i.e. typical cellular solid mechanical behaviour under compression e.g. initial response, plateau region, and densification.

4. Discussion

This study aimed to establish a new and novel pathway that generated TPE AM material model coefficients directly from experimental data, presenting an efficient and valid route to achieve accurate FE simulations than those previously described in the literature [19]. This pathway should encourage greater industrial uptake of new and existing TPE AM materials, enabling designing of higher-performance components.

A novel aspect of this study was the performance of tensile testing across low, medium and high strain-rates, quantifying the high degree of rate-dependency and anisotropy due to LS TPE's complex mechanical behaviour. Classical highly non-linear elastomer-like behaviour was observed. For purely uniaxial tension under a large monotonic deformation regime, a small period of initial stiffness was followed by a large softening region, under large strains. Trends varied across build orientation, with a clear hierarchy observed - where 'xy' exhibits superior performance versus 'xz' and 'zy', which is consistent with other AM studies [27]. Effective bonding of adjacent powder particles within the same layer, as well as relative to the previous layer, appears paramount to achieving superior mechanical performance. By incorporating a greater number of build layers, the chemical bonding is weaker due to a relatively high thermal difference between the current and previous build layers, meaning inferior mechanical performance. Experimental characterisation techniques were also able to achieve isolated, homogenous strain, with the TPE demonstrating significantly different behaviour in uniaxial, planar and equibiaxial tension. The TPE's mechanical behaviour was consistent with other elastomer-like materials, indicating that augmentation of a hyperelastic and linear viscoelastic material model is necessary to accurately mimic its complex mechanical behaviour [1].

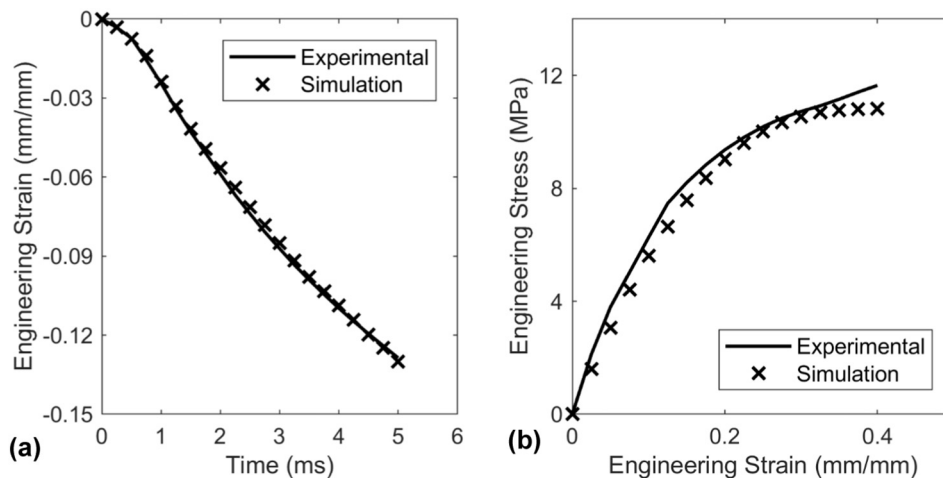


Fig. 8. Validation of HE and LVE material model for an isolated deformation mode, comparison of high strain rate tensile loading data against simulation: (a) nominal longitudinal strain-time history and, (b) current stress-strain behaviour.

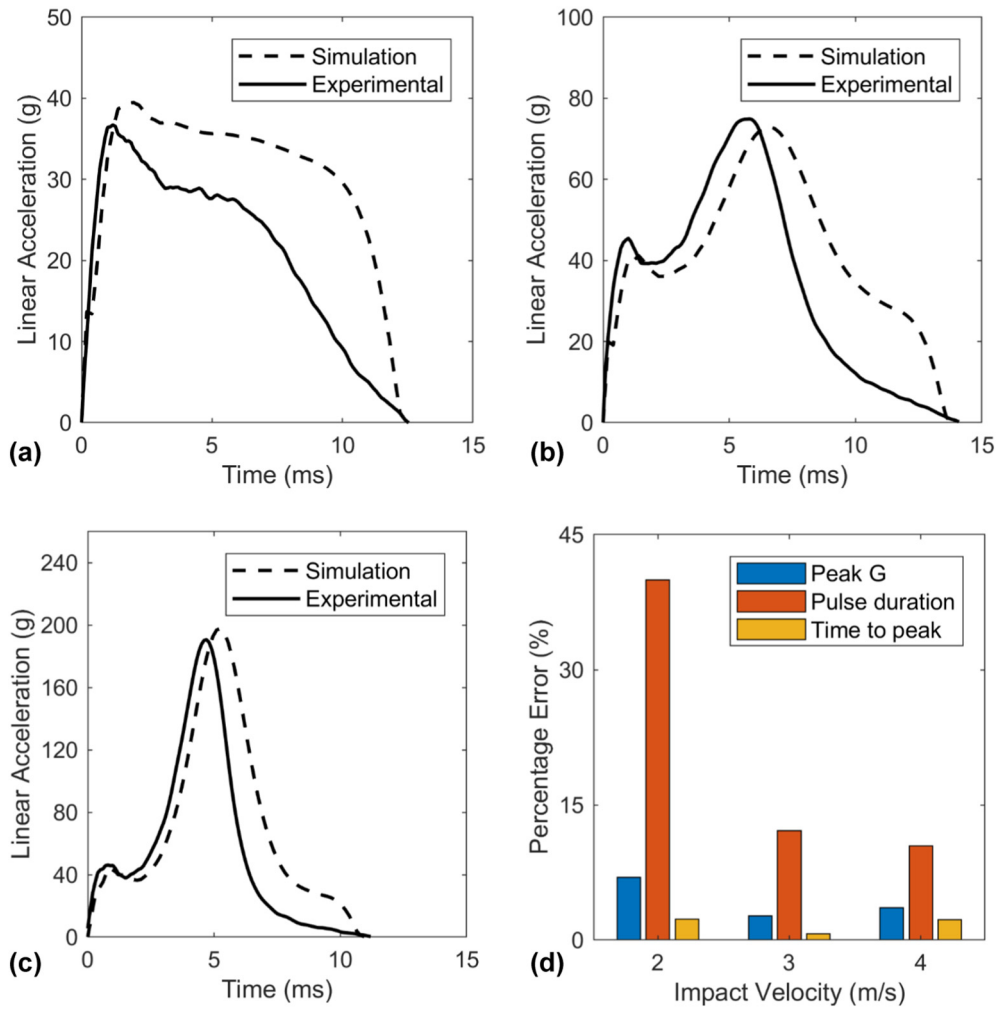


Fig. 9. Validation of HE and LVE material model for a mixed deformation mode, comparison of dynamic impact test data against simulation: (a) 2 m/s, (b) 3 m/s, (c) 4 m/s and (d) percentage error.

The Abaqus solver enabled comparison of different constitutive material models using the same experimental data input. The conditions of a relatively simple hyperelastic model were considered [28] to aid in selecting the most appropriate model, whilst the predictive capability in isolated and mixed deformation modes was assessed through total relative difference when comparing hyperelastic models. The Ogden $N = 5$ model is known to be easy to calibrate when using data from multiple tests [29], here presenting the least total relative difference versus the experimental data; however, it is computationally expensive [30]. The Van Der Waals model utilised significantly fewer coefficients, whilst demonstrating the second most favourable fit from the experimental data. The high degree of accuracy demonstrated by the Ogden $N = 5$ model provides the foundation for investigation within the dynamic regime when undergoing large deformation. The low RMS error requirement applied to the linear viscoelastic model solver implemented by Abaqus, results in the Prony series strongly agreeing with the experimental data. FE simulation using the defined material model coefficients compared accurately to experimental behaviour for a given strain range; therefore, it is anticipated similar accuracy would be found within a dynamic regime in the same range (± 0.5) for both isolated and mixed deformation modes.

Strong comparability was evident between the experimental and simulation in both isolated and mixed deformation states, demonstrating the validity of the presented pathway. For the isolated deformation state simulation (i.e. uniaxial tension), engineering stress and through-

thickness engineering strain (ε_{zz}) in the time domain were both accurately predicted, demonstrating the effectiveness of the calibrated material model in a state independent of geometry, negating any associated dynamic structural inertial effects. It is postulated that similar behaviour would also be observed for both planar and equibiaxial tension, although current experimental setups prohibit such testing and so this merits future investigation. For the mixed deformation state simulation (i.e. lattice-based impact), better comparison was observed in the initial loading phase (until densification), though the unloading phase was less favourable. This is probably due to the macro-structural behaviour of the lattice dominating the initial impact response, where the observed buckling behaviour was consistent with previous data [25]; however, in the unloading phase, the structural behaviour dominates less and the complex behaviour of the base material is more pronounced. Non-linear hyperelastic Mullins effect and viscoelastic hysteresis [1] behaviour during dynamic cyclic loading contribute to the prominence of lag, which is not captured by the proposed pathway for material model calibration. Considering the prominence of these phenomena, however, the overall dynamic response characteristics, such as peak acceleration and time duration, were all simulated to within 15% of the experimental data, across each loading regime. It is also important to note that more complex material models do exist. Viscoplastic models [1] may better capture the aforementioned phenomena, although are not widely available in FE software and they also require extensive data sets, which may not be required to

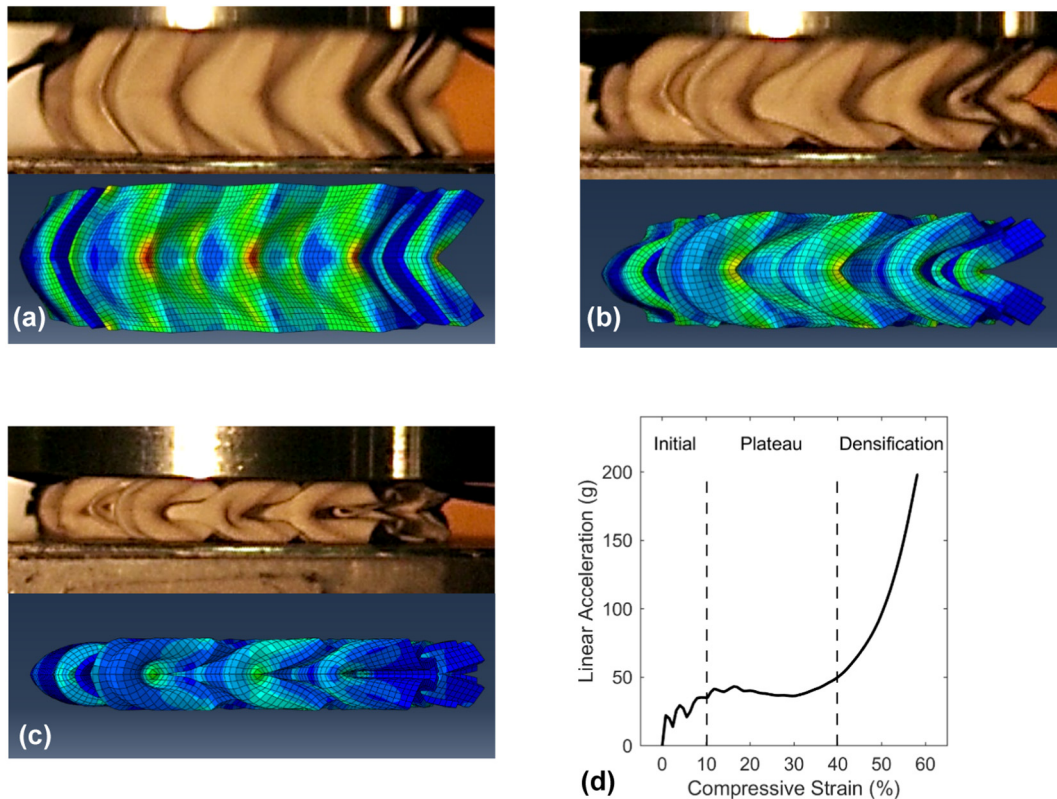


Fig. 10. Comparison of FE and experimental (2000 FPS) 'MO' lattice kinematic behaviour: (a) initial response, (b) plateau, (c) densification and (d) simulated acceleration-strain plot for 4 m/s impact.

accurately simulate the application, e.g. multi-use, elastically recoverable energy-absorbing structures.

This study captured the time-dependent behaviour for linear viscoelastic calibration using stress relaxation experiments. Stress relaxation experiments cannot achieve an instantaneous step input and will always include an initial loading ramp, as well as inertial effects from the test equipment loading. This is, however, compensated for by analysing the data and back-calculating to a theoretical instantaneous load point, an approach demonstrated here and in a previous study [21]. An alternative method is to utilise resonance methods, e.g. Dynamic Mechanical Analysis, which also captures the viscoelastic behaviour for strain-rates in a range near that of the impact. It is, however, equally as susceptible to the incorporation of user and/or analytical error, due to the utilisation of shift factors.

5. Conclusion

This study presents a novel process for efficiently characterizing materials used in transient, dynamic applications. Deriving model coefficients via uniaxial, planar and equibiaxial data, followed by validation in isolated and mixed deformation states at a range of strain rates, provides an efficient pathway to perform accurate FE simulations of TPE AM materials. These achievements mean this study provides a platform for engineers and designers to better exploit TPE AM materials, creating opportunities to develop the next generation of high-performance components.

Acknowledgements

This work was facilitated by a Royal Society Newton International Exchanges award (ref.: NI150260). M. Robinson was supported by the Knowledge Economy Skills Scholarships 2 (via the Welsh Government's European Social Fund).

CRedit authorship contribution statement

Rhosslyn Adams: Methodology, Validation, Formal analysis, Investigation, Writing - original draft, Visualization. **Shwe P. Soe:** Conceptualization, Validation, Supervision. **Rafael Santiago:** Methodology, Investigation, Resources. **Michael Robinson:** Methodology, Writing - review & editing. **Benjamin Hanna:** Writing - review & editing. **Graham McShane:** Conceptualization. **Marcilio Alves:** Conceptualization, Resources, Funding acquisition. **Roy Burek:** Resources. **Peter Theobald:** Conceptualization, Writing - review & editing, Supervision, Project administration, Funding acquisition.

References

- [1] J. Bergström, *Mechanics of Solid Polymers*, Elsevier, 2016.
- [2] F.N. Habib, P. Iovenitti, S.H. Masood, M. Nikzad, Fabrication of polymeric lattice structures for optimum energy absorption using Multi Jet Fusion technology, *Mater. Des.* 155 (2018) 86–98 Oct.
- [3] S.R.G. Bates, I.R. Farrow, R.S. Trask, 3D printed polyurethane honeycombs for repeated tailored energy absorption, *Mater. Des.* 112 (2016) 172–183 Dec.
- [4] T. Li, Y. Chen, X. Hu, Y. Li, L. Wang, Exploiting negative Poisson's ratio to design 3D-printed composites with enhanced mechanical properties, *Mater. Des.* 142 (2018) 247–258 Mar.
- [5] C. Yang, H.D. Vora, Y. Chang, Behavior of auxetic structures under compression and impact forces, *Smart Mater. Struct.* 27 (2) (2018), 025012 Feb.
- [6] S.P. Soe, N. Martindale, C. Constantinou, M. Robinson, Mechanical characterisation of Duraform® Flex for FEA hyperelastic material modelling, *Polym. Test.* 34 (2014) 103–112 Apr.
- [7] S.P. Soe, D.R. Evers, R. Setchi, Assessment of non-uniform shrinkage in the laser sintering of polymer materials, *Int. J. Adv. Manuf. Technol.* 68 (1–4) (2013) 111–125 Sep.
- [8] S.P. Soe, Quantitative analysis on SLS part curling using EOS P700 machine, *J. Mater. Process. Technol.* 212 (11) (2012) 2433–2442.
- [9] S.H. Huang, P. Liu, A. Moksadar, L. Hou, Additive manufacturing and its societal impact: a literature review, *Int. J. Adv. Manuf. Technol.* 67 (5–8) (2013) 1191–1203 Jul.
- [10] D. W. Abueidda, M. Elhebeary, C.-S. (Andrew) Shiang, S. Pang, R. K. Abu Al-Rub, and I. M. Jasiuk, "Mechanical properties of 3D printed polymeric Gyroid cellular structures: experimental and finite element study," *Mater. Des.*, vol. 165, p. 107597, Mar. 2019.

- [11] D.W. Abueidda, M. Bakir, R.K. Abu Al-Rub, J.S. Bergström, N.A. Sobh, I. Jasiuk, Mechanical properties of 3D printed polymeric cellular materials with triply periodic minimal surface architectures, *Mater. Des.* 122 (2017) 255–267 May.
- [12] W. Zhu, C. Yan, Y. Shi, S. Wen, J. Liu, Y. Shi, Investigation into mechanical and microstructural properties of polypropylene manufactured by selective laser sintering in comparison with injection molding counterparts, *Mater. Des.* 82 (2015) 37–45 Oct.
- [13] S. Yuan, F. Shen, J. Bai, C.K. Chua, J. Wei, K. Zhou, 3D soft auxetic lattice structures fabricated by selective laser sintering: TPU powder evaluation and process optimization, *Mater. Des.* 120 (2017) 317–327 Apr.
- [14] J.F. Christ, N. Aliheidari, A. Ameli, P. Pötschke, 3D printed highly elastic strain sensors of multiwalled carbon nanotube/thermoplastic polyurethane nanocomposites, *Mater. Des.* 131 (2017) 394–401 Oct.
- [15] P. Sun, L. Zhang, S. Tao, Preparation of hybrid chitosan membranes by selective laser sintering for adsorption and catalysis, *Mater. Des.* 173 (2019), 107780 Jul.
- [16] M. Robinson, S. Soe, G. McShane, R. Celeghini, R. Burek, M. Alves, B. Hanna, P. Theobald, Developing elastomeric cellular structures for multiple head impacts, IRCOB conference 2017, 2017.
- [17] Y. Wang, L. Zhang, S. Daynes, H. Zhang, S. Feih, M.Y. Wang, Design of graded lattice structure with optimized mesostructures for additive manufacturing, *Mater. Des.* 142 (2018) 114–123 Mar.
- [18] J. Zhao, M. Zhang, Y. Zhu, X. Li, L. Wang, J. Hu, A novel optimization design method of additive manufacturing oriented porous structures and experimental validation, *Mater. Des.* 163 (2019), 107550 Feb.
- [19] Y. Han, W. Lu, C. Yang, H.D. Vora, Y. Chang, Evolutionary design of nonuniform cellular structures with optimized Poisson's ratio distribution, *Mater. Des.* 141 (2018) 384–394 Mar.
- [20] J.E. Ryu, E. Salcedo, H.J. Lee, S.J. Jang, E.Y. Jang, H.A. Yassi, D. Baek, D. Choi, E. Lee, Material models and finite analysis of additively printed polymer composites, *J. Compos. Mater.* 53 (3) (2019) 361–371 Feb.
- [21] M. Robinson, S. Soe, R. Johnston, R. Adams, B. Hanna, R. Burek, G. McShane, R. Celeghini, M. Alves, P. Theobald, Mechanical characterisation of additively manufactured elastomeric structures for variable strain rate applications, *Addit. Manuf.* 27 (2019) 398–407 May.
- [22] ASTM International, Standard Test Method for Tensile Properties of Plastics, D638 - 14, 2002.
- [23] R. Santiago, W. Cantwell, M. Alves, Impact on thermoplastic fibre-metal laminates: experimental observations, *Compos. Struct.* 159 (2017) 800–817 Jan.
- [24] B. Standard, I.S.O., & ISO, Rubber, Vulcanized or Thermoplastic – Determination of Compression Stress-strain Properties, 2005.
- [25] M. Schenk, S.D. Guest, G.J. McShane, Novel stacked folded cores for blast-resistant sandwich beams, *Int. J. Solids Struct.* 51 (25–26) (2014) 4196–4214 Dec.
- [26] K. Miura, *The Science of Miura-ori: A Review*. A K Peters, 2009.
- [27] G. Berti, L. D'Angelo, A. Gatto, L. Iuliano, Mechanical characterisation of PA-Al₂O₃ composites obtained by selective laser sintering, *Rapid Prototyp. J.* 16 (2) (2010) 124–129 Mar.
- [28] G. Chagnon, G. Marckmann, E. Verron, A comparison of the Hart-Smith model with Arruda-Boyce and Gent formulations for rubber elasticity, *Rubber Chem. Technol.* 77 (4) (2004) 724–735 Sep.
- [29] A. Ali, M. Hosseini, B.B. Sahari, A. Ali, M. Hosseini, B.B. Sahari, A review of constitutive models for rubber-like materials, *Am. J. Eng. Appl. Sci.* 3 (1) (2010) 232–239 Jan.
- [30] M. Forni, A. Martelli, A. Dusi, Implementation and Validation of Hyperelastic Finite Element Models of High Damping Rubber Bearings, Sep 1999.